Journal of Ceramic Processing Research. Vol. 10, No. 4, pp. 548~552 (2009)

JOURNAL OF
Ceramic Processing Research

Photo-catalysis of phenol derivatives with Fe_2O_3 nanoparticles dispersed on SBA-15

E. Montiel-Palacios[a], A. K. Medina-Mendoza[b], A. Sampieri[c], C. Angeles-Chávez[d], I. Hernández-Pérez[b] and R. Suarez-Parra[a,*]

[a]*Departamento de Materiales Solares, Centro de Investigación en Energía de la UNAM, Priv. Xochicalco s/n, 62580, Temixco Mor., Mexico*

[b]*Universidad Autónoma Metropolitana-A, Dpto. de Ciencias Básicas, Av. Sn. Pablo No. 180, México 02200, D. F., Mexico*

[c]*Colegio de Postgraduados, Campus Montecillo, Carretera México-Texcoco, km 36.5, 56230, Montecillo, Estado de México, Mexico*

[d]*Instituto Mexicano del Petróleo, Programa de Ingeniería Molecular, Eje Central Lázaro Cárdenas 152, 07730 México, D. F. Mexico*

Highly ordered hexagonal (*p6mm*) mesoporous silica SBA-15 was synthesized through a hydrothermal treatment under acidic conditions. Fe_2O_3/SBA-15 catalysts were prepared by impregnation of SBA-15 media with iron(III) acetylacetonate, iron(III) chloride or iron(II) sulfate solutions. X-ray Diffraction (XRD), X-ray fluorescence (XRF), high angle annular dark field scanning transmission electron microscopy (HAADF-STEM), energy dispersive X-ray (EDX) spectroscopy and nitrogen physisorption characterization were carried out for SBA-15 and Fe_2O_3/SBA-15 materials. After impregnation and calcination at 823 K, the iron oxide dispersion in SBA-15 was analyzed by STEM and EDX. $FeCl_3$ provides the highest amount of Fe loading in mesoporous SBA-15. The photocatalytic properties of Fe_2O_3/SBA-15 samples at pH = 3 and pH = 6 were evaluated in catechol and hydroquinone photodecomposition by inducing visible radiation. The conversion of catechol and hydroquinone, at pH = 3 and pH = 6 with iron(III) acetylacetonate and $FeCl_3$ as the precursor of iron oxide nanoparticles, were measured by UV-Vis spectroscopy, chemical oxygen demand (COD) and total organic carbon (TOC) analysis.

Key words: SBA-15, Nanoparticles of iron oxide, Photocatalysis, Catechol.

Introduction

Phenol and its derivatives represent a dangerous environmental problem in industrial wastewaters due to their high toxicity, i.e. hydroquinone and catechol. Unfortunately, biological degradation processes cannot be carried out due to bactericidal character of phenol compounds. To avoid this problem, different studies propose semiconductor materials to eliminate phenol derivates through heterogeneous photocatalytic reactions, for instance, irradiated solid semiconductors provide available charges (electrons and positive holes) indispensable in the redox processes of both organic and inorganic contaminants. The TiO_2 is a good example of a semiconductor material, which has been extensively studied in different redox processes however, it is a non-porous material with a low surface area and it needs to be irradiated by a UV light source to eliminate organic compounds.

Therefore various porous materials have been used and evaluated as catalyst supports to study their catalytic and photo-catalytic properties in order to improve phenol decomposition. For instance, the catalytic properties of metal supported materials can be improved using mesoporous supports, such as MCM-41 or SBA-15. Indeed, mesoporous materials have large surface area with a controlled pore size, and these characteristics make them promising supports to prepare catalysts for photocatalysis of wastewater.

For catalytic purposes the SBA-15 has been grafted with different metals or metal oxides [1-7], while iron(II/III) solutions, iron oxohydroxides and iron oxides, have been tested either as homogeneous or heterogeneous catalysts to eliminate phenol or its derivatives in wastewater [8-12].

In this study catechol and hydroquinone are proposed as phenol derivates and they are decomposed using the following photocatalytic system: Fe_2O_3/SBA-15, hydrogen peroxide and visible radiation. Iron acetylacetonate-$Fe(C_5H_7O_2)_3$, iron chloride-$FeCl_3$ and iron sulfate- $FeSO_4$ are the precursors used to study the loading role of Fe supported on SBA-15.

Experimental Procedures

A silica mesopourous support, SBA-15, was synthesized using a triblock copolymer, Pluronic P123 ($EO_{20}PO_{70}EO_{20}$ Basf Aldrich) as direct-structuring agent [13]. The silica source was the Tetraethyl orthosilicate (TEOS, 98% Sigma-Aldrich). First of all, the Pluronic P123 (16 g) was mixed with 474 ml of HCl (2 M), in a teflon bottle. The resulting mixture was agitated for one hour at 298 K and then heated at 311 K in a bain-marie until dissolution of the structuring agent. Then, 32 g of TEOS was added to the mixture which was maintained at 311 K for 24 hours, under maximum

*Corresponding author:
Tel : (52) 5622-9820
Fax: (52) 5622-9820
E-mail: rsp@cie.unam.mx

stirring conditions. Subsequently, the mixture was heated at 368 K in an oven for 72 hours. The solid obtained was filtered and washed with abundant deionized water. Finally, the solid SBA-15 was calcined at 823 K for 6 hours, with a 1 K minute^{-1} heating rate, to remove the structuring agent and liberate the porosity.

In order to prepare the catalysts, 3 g of the SBA-15 were impregnated with 3 wt% of Fe in a volume of 100 ml of ethanol (purity 99%) through a solution of Fe(III)-acetylacetonate [$Fe(C_5H_7O_2)_3$, 0.016 M]. After stirring at 298 K for 3 hours, the resulting mixture was filtered and washed with ethanol. Besides, the impregnation of SBA-15 with iron inorganic salts, $FeCl_3$ and $FeSO_4$, was carried out following the same procedure but in aqueous solutions. The impregnated samples were calcined at 823 K for 6 hours, with a 1 K minute^{-1} heating rate.

Characterization Methods

XRD measurements at low angles were scanned at 0.5/2θ in a Siemens D-500 apparatus with Cu K_α radiation (wavelength $\lambda = 1.5428$ Å), in order to corroborate the synthesis of SBA-15. XRD diffractograms at high angles were collected in a Rigaku DMAX 2200 apparatus to detect peaks assigned to iron oxide in Fe_2O_3/SBA-15 catalysts.

A Philips MagiX PRO X-ray fluorescence spectrometer (XRF) with a Rh anode was used to determine the iron amount in the SBA-15 support. The XRF spectra were recorded using a LiF (200) crystal, (2d = 0.403 nm) for the Fe-$K_{\alpha 1,2}$ fluorescence line (2θ = 57.479).

Scanning transmission electron microscopy (STEM) analyses were performed in a JEM-2200FS transmission electron microscope with an accelerating voltage of 200 kV and images were acquired by a HAADF detector. Local chemical analysis by energy dispersive X-ray (EDX) spectrometry was performed in a NORAN energy dispersive X-ray spectroscope in order to identify the presence of iron in the SBA-15. The samples were ground, suspended in isopropanol at room temperature, and dispersed with ultrasonic agitation; then a drop of the solution was placed on a 3 mm diameter carbon film supported on a holey copper grid.

Nitrogen adsorption-desorption isotherms were measured at 77 K using a NOVA 1200e surface area and pore size analyzer (Quantachrome). Before analysis the samples were outgassed at 473 K for 16 hours. The BET method was used to calculate the surface area and the average pore size was evaluated by BJH model.

Each photocatalytic experiment was carried out with 0.1 g of catalyst in 0.5 dm^3 of an organic compound solution containing 100 ppm of catechol or hydroquinone. UV absorbance, COD and TOC analysis were measured in a Hach DR-5000 Spectrophotometer. Visible radiation used in the photocatalytic system was provided by a 100 W/m^2 domestic white lamp, similar to the system used in [14]. The photolysis of organic compounds was not detected by UV spectrophotometry during five hours of reaction.

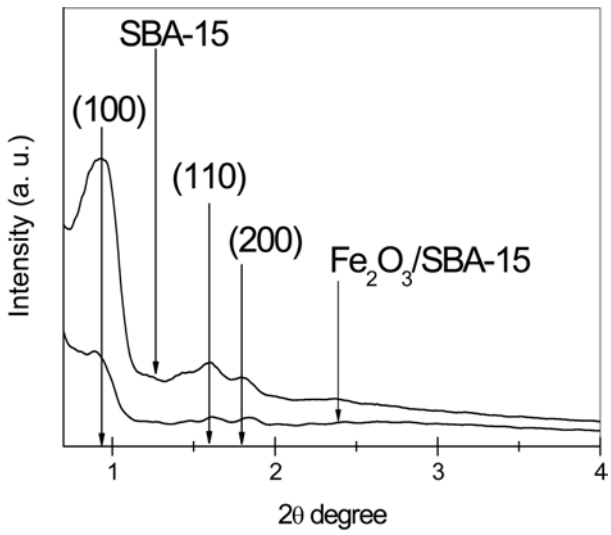

Fig. 1. XRD patterns of SBA-15 and Fe_2O_3/SBA-15 (with $Fe(C_5H_7O_2)_3$ as the precursor) in the low angle range.

Results and Discussion

The XRD pattern of the system Fe_2O_3/SBA-15, in the low angle range, shows the main three characteristic peaks (100), (110) and (200) corresponding to the SBA-15, Fig. 1. This result suggests that the hexagonal structure of SBA-15 is preserved after the impregnation with the Fe_2O_3 compound. However, the peaks intensities decrease after Fe loading, which could be explained due to the fact that Fe is a strong X-ray absorber. At the same time, in the XRD pattern of the system Fe_2O_3/SBA-15 is also clearly seen that the original position of the three peaks has been changed. In the three cases the shift is lower than one degree but, even though the change is too small, the displacement of the three diffraction peaks (100), (110) and (200) indicates that the lattice parameters of the SBA-15 have been modified by the presence of iron oxide nanoparticles on its surface and, maybe, in its porous.

TEM images in Fig. 2a and 2b also confirm that mesoporous silica SBA-15 has a highly ordered hexagonal (*p6mm*) structure. In other hand, the analyses of STEM images have permitted to acquire the following results, concerning to the iron catalysts. If the $Fe(C_5H_7O_2)_3$ is the iron oxide precursor, after calcination at 823 K, some spots are observed on the surface of the SBA-15, Figs. 2c and 2d. Besides, EDX microanalysis, Fig. 2, confirm that Fe is detected on the surface of the SBA-15, hence these spots may be attributed to Fe_2O_3 nanoparticles. However, if $FeCl_3$ is used as the precursor of Fe_2O_3 nanoparticles, the spots on the support surface are more difficult to observe, Figs. 3a and 3b. Despite this result, EDX microanalysis, Fig 3, show that Fe can be sporadically detected on the surface of SBA-15. Finally, if a solution of $FeSO_4$ is impregnated on SBA-15 there are not spots on the surface Figs. 3c and 3d, and no Fe could be detected by EDX, Fig. 3.

XRF analyses were measured in order to determine the real Fe loading in the Fe_2O_3/SBA-15 catalysts. As indicated

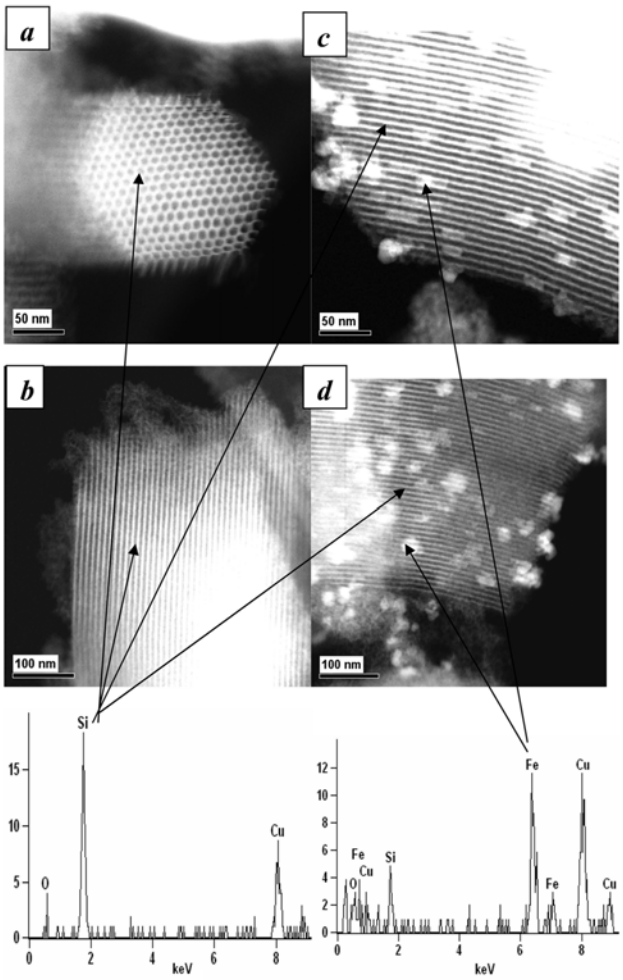

Fig. 2. HAADF-STEM images of SBA-15 (*a, b*) and Fe_2O_3/SBA-15 (*c, d*) $Fe(C_5H_7O_2)_3$ as the precursor, and EDX spectra performed on the support and white spots.

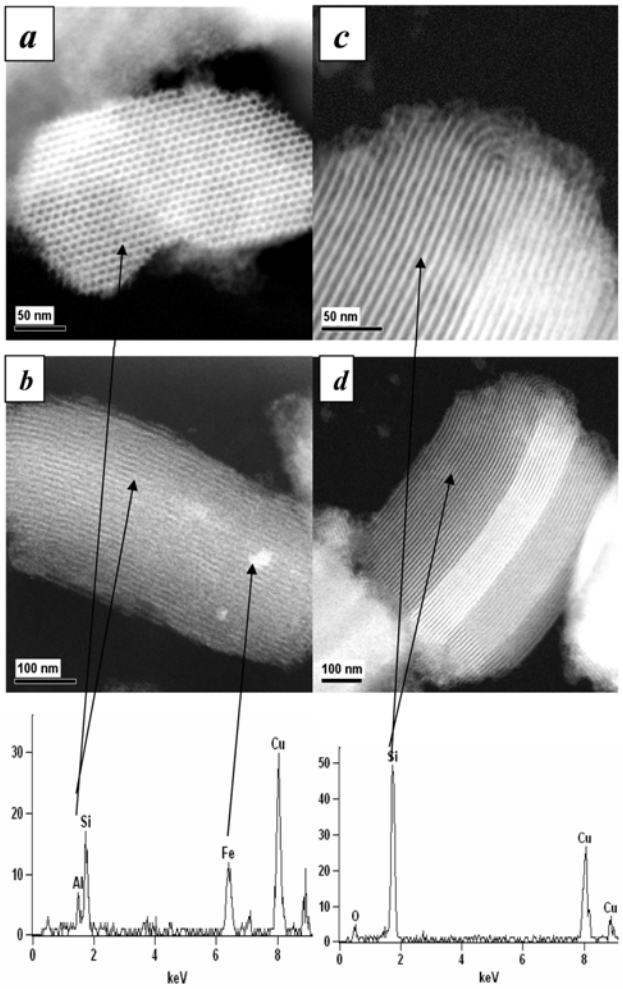

Fig. 3. HAADF-STEM images of Fe_2O_3/SBA-15, where Fe_2O_3 was prepared with $FeCl_3$ (a, *b*) and $FeSO_4$ (*c, d*) and EDX spectra in white spots and support.

in Table 1, the amount of Fe is different in the three samples; the highest amount is reached when $FeCl_3$ is used as the precursor, 1.1 wt%, whereas only 0.14 wt% of Fe is detected on the SBA-15, with $FeSO_4$ as the precursor. In contrast, an intermediate amount of Fe, 0.55 wt%, is attained using $Fe(C_5H_7O_2)_3$ during impregnation of SBA-15.

Results obtained previously show that the dispersion degree of Fe_2O_3 nanoparticles on the surface of SBA-15 is strongly dependent on the Fe precursor: $FeSO_4$ > $FeCl_3$ > $Fe(C_5H_7O_2)_3$. Although Fe_2O_3 nanoparticles are very difficult to observe by TEM, due to the poor contrast difference between SBA-15 and iron oxides particles, the EDX analyses suggest that Fe_2O_3 nanoparticles may be dispersed, also, into the channels of SBA-15, mainly for $FeCl_3$ precursor.

The N_2 adsorption-desorption isotherms of both support and catalyst are displayed in Fig. 4. Type IV isotherms with H1 hysteresis loops are observed in SBA-15 and Fe_2O_3/SBA-15 (with $Fe(C_5H_7O_2)_3$ as the precursor), which are typical isotherms of mesoporous materials. Table 1 compares the BET area and average pore size of samples prepared with the three Fe precursors. Although SBA-15 and Fe_2O_3/SBA-15 catalysts (with $Fe(C_5H_7O_2)_3$, $FeCl_3$ or $FeSO_4$ precursors) show similar surface areas, around 600 m^2/g, the SBA-15 pore size distribution decreases after Fe loading, around 0.6 nm. The relatively low concentration of Fe (0.14-1.10%) leads to have similar surface areas as the starting material. Besides, the pore size variation between the support and the catalysts could also be explained due to the recalcination of catalysts after the impregnation procedure.

Table 1. Iron amount in Fe_2O_3/SBA-15 systems using different iron salts and their textural properties

Precursor source	*Fe real amount (wt %)	BET surface (m^2/g)	Pore size (nm)
SBA-15	0.00	610	6.6
$Fe(C_5H_7O_2)_3$	0.55	610	6.2
$FeCl_3$	1.10	590	6.0
$FeSO_4$	0.14	590	6.0

*Fe amounts were determined by XRF with a square correlation of r^2 = 0.9969

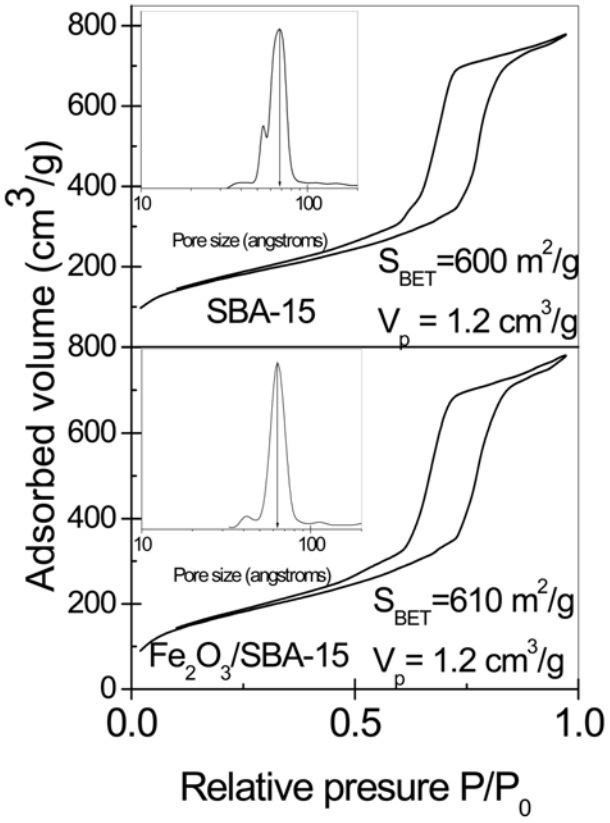

Fig. 4. Nitrogen adsorption/desorption isotherm and pore size distribution of SBA-15 and Fe_2O_3/SBA-15.

Photodegradation Catalysis

The photodegradation performance of catechol and hydroquinone were measured at 276 and 289 nm, since these are the maximum intensity peaks observed by UV spectroscopy for both organic compounds.

The Fe_2O_3/SBA-15 catalyst, prepared through $FeSO_4$ impregnation, is not considered in the following figures due to the relatively small amount of Fe and, therefore, a low conversion of catechol and hydroquinone (both 20%). Instead, if $Fe(C_5H_7O_2)_3$ is the precursor of the iron oxide nanoparticles, 50% of catechol and 90% of hydroquinone conversion are attained after 300 minutes of reaction at pH = 3, Fig. 5. On the other hand, the Fe_2O_3/SBA-15 catalyst (with $FeCl_3$ as the precursor of the iron oxide nanoparticles) leads to 90% and 98% of conversion for catechol and hydroquinone, respectively (Fig. 5). Of course, this catalyst show a higher conversion because the amount of Fe is 1.1%, twice higher than the catalyst prepared with $Fe(C_5H_7O_2)_3$. The high conversion of both organic compounds using $FeCl_3$ as the precursor of Fe_2O_3 could also be influenced by a highly active catalytic surface of this Fe_2O_3/SBA-15 system. Indeed, iron oxide nanoparticles observed by STEM suggest a wide dispersion on the surface and in the porous matrix of the mesostructured SBA-15, also contributing to an excellent photocatalytic performance.

Furthermore, if the pH = 6, the conversion of catechol and hydroquinone is increased by reducing the time contact

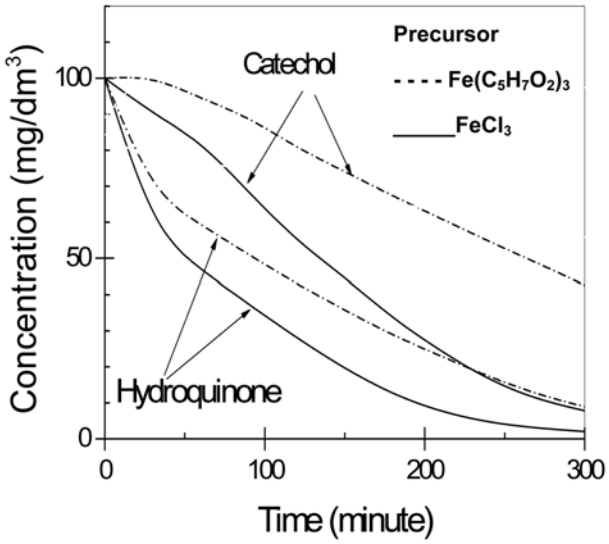

Fig. 5. Evolution of the catechol and hydroquinone concentration during the photodegradation process with Fe_2O_3/SBA-15 (precursors $FeCl_3$ and $Fe(C_5H_7O_2)_3$) as a function of time at pH = 3.

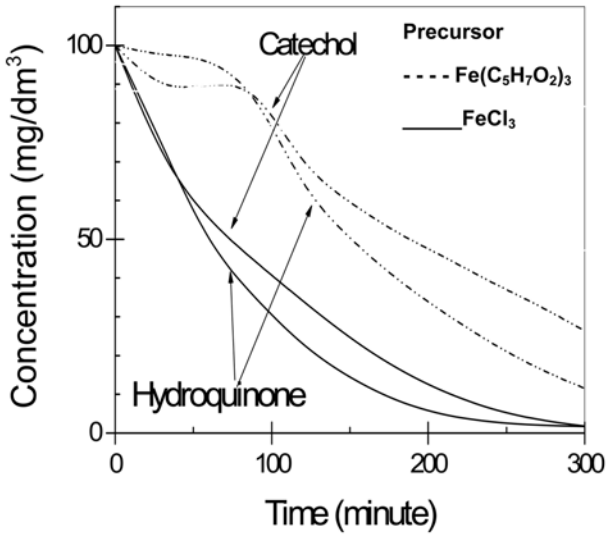

Fig. 6. Evolution of the catechol and hydroquinone concentration during the photodegradation process with Fe_2O_3/SBA-15 (precursors $FeCl_3$ and $Fe(C_5H_7O_2)_3$) as a function of time at pH = 6.

in the photocatalytic process, Fig. 6. The catechol conversion using Fe_2O_3/SBA-15 ($Fe(C_5H_7O_2)_3$ as the precursor) reaches 70%. The hydroquinone conversion in this system is delayed at the beginning of the degradation process but similar to the case of pH = 3 the conversion reaches 90%. As expected, the increasing of conversion is more evident in the Fe_2O_3/SBA-15 catalyst with $FeCl_3$ as the precursor of iron oxide nanoparticles, since catechol and hydroquinone show similar trends, both with more than 90% of conversion after 240 minutes of reaction, Fig. 6.

The results obtained from the photocatalytic process also indicate that, by increasing the iron concentration in the SBA-15 the photocatalytic activity is improved due to a high generation of hydroxyl (•OH) species from hydrogen peroxide, as the reduction process of hydrogen peroxide

Table 2. Results of COD and TOC analyses at the beginning and at the end of the catechol photodegradation process with Fe_2O_3/SBA-15 and hydrogen peroxide.

pH/precursor of iron oxide	COD_i mg/dm^3 O_2	COD_f mg/dm^3 O_2	TOC_i mg/dm^3 C	TOC_f mg/dm^3 C
3/$FeCl_3$	540	400	39	18
3/ $Fe(C_5H_7O_2)_3$	540	500	44	30
6/ $FeCl_3$	530	420	44	20
6/ $Fe(C_5H_7O_2)_3$	550	500	43	30

Table 3. Results of COD and TOC analyses at the beginning and at the end of the hydroquinone photodegradation process with Fe_2O_3/SBA-15 and hydrogen peroxide.

pH/precursor of iron oxide	COD_i mg/dm^3 O_2	COD_f mg/dm^3 O_2	TOC_i mg/dm^3 C	TOC_f mg/dm^3 C
3/$FeCl_3$	490	390	40	17
3/ $Fe(C_5H_7O_2)_3$	520	440	55	23
6/ $FeCl_3$	490	400	38	20
6/ $Fe(C_5H_7O_2)_3$	550	480	48	27

molecules depends on the visible light interaction with the iron oxide surface. The influence of pH = 6 could be mainly related to changes in the solvate process. In fact, the concentration of hydronium ions (H_3O^+) diminishes at pH = 6, catechol and hydroquinone molecules are exempted by the screening effect of the hydronium ions. Therefore, the chemical adsorption of catechol and hydroquinone molecules increases on the iron oxide surfaces.

Although the disappearance of the absorption bands at 276 and 289 nm (catechol and hydroquinone respectively) in the UV absorbance spectra suggest a decrease in the toxicity of the samples, we have also determined the water quality by COD and TOC analysis, before and after photodegradation processes at pH = 3 and pH = 6. The changes in the COD and TOC values before and after the elimination of catechol and hydroquinone confirm their transformation on other types of organic soluble compounds. As can be seen in Table 2 and Table 3 the water quality has been improved after five hours of reaction.

Conclusions

Iron oxide nanoparticles were prepared by calcination on the surface and in the porous matrix of SBA-15 previously impregnated with an organic, $Fe(C_5H_7O_2)_3$ and two inorganic, $FeCl_3$ and $FeSO_4$, solutions. However, in the case of $FeSO_4$ precursor no greater loading of Fe was introduced after impregnation of SBA-15. The photocatalytic properties of Fe_2O_3/SBA-15 catalysts were assessed on catechol and hydroquinone compounds. Indeed, the amount and degree of dispersion of Fe on SBA-15 porosity, as well as the photocatalytic performances were strongly dependent of the precursor, i.e.: $FeCl_3 > Fe(C_5H_7O_2)_3 >>> FeSO_4$. The UV spectroscopy results depict a fast photodegradation process of catechol or hydroquinone at pH = 3 and pH = 6. However, it is still necessary to identify the products formed at the end of the reaction and to study the kinetics of the degradation process by HLPC.

Acknowledgments

Authors thank to Ma. Luisa-Ramón and L. Baños for the XRD analyses, P. Altuzar for the XRF analyses and R. Morán-Elvira for his assistance in the experiments. Authors also acknowledge DGAPA-UNAM for financial support concerning the projects IN215606, IN113003, IN114902; as well as CONACyT México-G38618-U, D.00446 IMP and FIES 98-47-III.

References

1. Ch. Yang, H. Lin and B. Zibrowius, Chem. Mater. 19 (2007) 3205-3211.
2. S. Lee, B. Park, S. Byeon and F. Chang, Chemistry of Materials 18[24] (2006) 5631-5633.
3. X.Q. Wang, H.L. Ge and Y.J. Cui, Microporous and Mesoporous Materials 86 (2005) 335-340.
4. T. Tsoncheva and J. Rosenholm, Microporous and Mesoporous Materials 89 (2006) 209-218.
5. Ch. Li, Y. Wang and Y. Guo, Chem. Mater. 19 (2007) 173-178.
6. R. Zhang, W. Ding, B. Tu and D. Zhao, Chemistry of Materials 19[18] (2007) 4379-4381.
7. Z. Wang, F. Zhang and Y. Yang, Chem. Mater 19 (2007) 3286-3293.
8. M. Rodríguez and S. Malato, Solar Energy 79 (2005) 360-368.
9. M-Ch. Lu, Chemosphere 40 (2000) 125-130.
10. D. Wang, Z. Liu, F. Liu and X. Ai, Applied Catalysis A: General 174 (1998) 25-32.
11. F. Martínez and G. Calleja, Applied Catalysis B: Environmental 60 (2005) 181-190.
12. F. Martínez and G. Calleja, Applied Catalysis B: Environmental 70 (2007) 452-460.
13. D. Zhao, Q. Huo, J. Feng, B.F. Chmelka and G.D. Stucky, J. Am. Chem. Soc. 120 (1998) 6024-6036.
14. R. Suárez Parra, I. Hernández Pérez and M.E. Rincón, Solar Energy Materials & Solar Cells 76 (2003), 189-199.